Integrated optical cross strip interferometer

Manfred Lohmeyer [*a], Remco Stoffer [a], Ludger Wilkens [b], Horst Dötsch [b]

[a] MESA$^+$ Research Institute, University of Twente,
P.O. Box 217, 7500AE Enschede, The Netherlands
[b] Department of Physics, University of Osnabrück,
Barbarastraße 7, D-49069 Osnabrück, Germany

ABSTRACT

A thick, bimodal segment of specific length and height between two single mode sections of a planar waveguide can serve as an integrated optical interferometer. It is realized by etching a wide strip from a guiding film. A — vertically guided, laterally unguided — beam of light is then made to traverse the strip perpendicularly. For a wide range of materials the structure can be dimensioned such that it shows the proper behaviour of an interferometer: Depending on the phase gain of the two modes in the thick region, the guided light interferes either almost completely destructively at the transition to the output segment, i.e. the power is radiated away into the substrate and cover regions, or constructively, i.e. most of the power passes the device. We believe that for certain applications structures of this kind can be a simple substitute for instruments like Mach-Zehnder interferometers or directional couplers. This is illustrated by two numerically simulated examples: A polarizer constructed from silicon based waveguides, which offers 30 dB polarization discrimination and 0.1 dB insertion loss with a total length of only 10 micrometers, and a proposal for an integrated magnetooptic isolator experiment, where the freedom in the lateral direction can be exploited for a proper tuning of the device.

Keywords: integrated optics, waveguide interferometer, polarizer device, magnetooptic isolator

1. INTRODUCTION

Interferometric devices like Mach-Zehnder structures or directional couplers form the basis for a variety of integrated optical instruments. Usually the inserted power is distributed between a number of relevant states, e.g. between the separate modes in the two arms of a Mach-Zehnder interferometer. After propagating along the device, these states interfere at the outlet, with the amount of the transferred power depending on their relative phases. Several interesting applications comprise only one relevant output port; here the terms constructive and destructive interference are applicable to characterize complete or vanishing power transmission.

This paper deals with a structure that can be considered as an alternative to the mentioned concepts. Figure 1 sketches the geometry. It can be viewed as a (vertical) two-dimensional directional coupler missing a gap, or as a multimode interference device involving only two modes. Despite its simplicity, the configuration shows the characteristic features of an interferometer. At the first junction ($z = 0$ in Figure 1), the power inserted via the single guided mode of the thin input segment is distributed among the two guided modes of the subsequent thick region. The two modes propagate across the strip. At the output junction (at $z = L$), their superposition excites the single mode of the output segment. While it is obvious that the transmitted power depends somehow on the relative phase of the two incoming fields, the quality of this dependence is quite surprising. Provided that the layer thicknesses and the etching depth are carefully selected, the output power can vanish entirely for a specific relative phase, while for another value more than 99 % of the input power pass the device. A simple overlap model, given in Section 2, is sufficient to explain these findings. The section includes a numerical verification by means of less approximate simulations, details of which can be found in Ref. 1.

Section 3 reports on the enhancement of the interferometer performance with respect to loss reduction by using the double layer configuration of Figure 1. We show that proper adjustment of the layer thicknesses and etching depth can enable the destructive interference property for a wide range of material parameters. The remaining two sections 4 and 5 sketch two applications of the "cross strip" concept, a double layer polarizer, that exhibits less insertion loss than the single layer configuration of Ref. 1, and a proposal for an easily tunable isolator experiment. Details on the latter are given in Ref. 2.

* Phone: +31/53/489-3448, Fax: +31/53/489-4833, E-mail: m.lohmeyer@math.utwente.nl

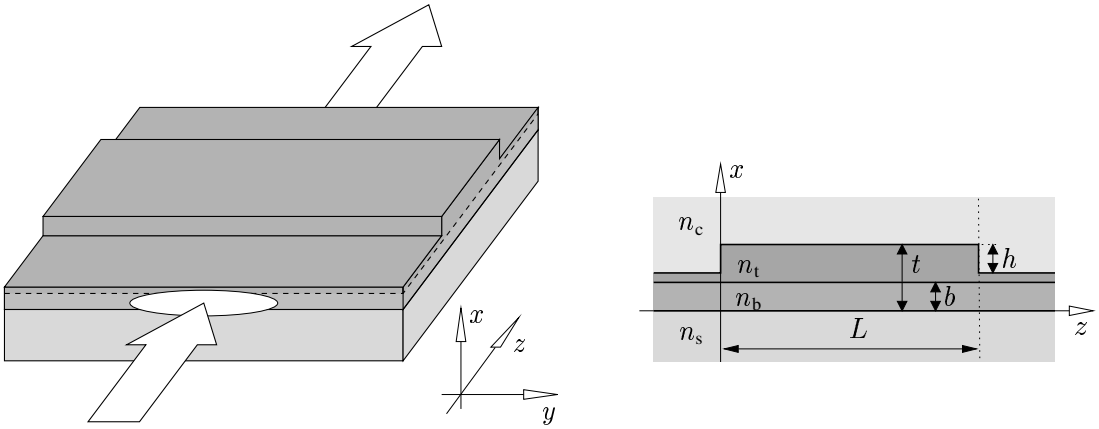

Figure 1. The planar waveguide geometry. x and y are the cross section coordinate axes, with the x-direction normal to the film plane. Light propagates along the z-direction, perpendicularly to a wide strip that has been etched into the guiding film. n_s, n_b, n_t, and n_c are the refractive indices of the substrate, the bottom and top film layer, and the cover; t, b, h, and L denote the total film thickness, the thickness of the bottom layer, the etching depth, and the strip width (the length of the thick segment), respectively.

2. CROSS STRIP INTERFEROMETER

Assuming a vanishing y-dependence of the permittivity and of the electromagnetic fields, the cross strip is to be modeled in a strictly 2–D setting. For fixed vacuum wavelength λ, all parameters introduced in the caption of Figure 1 shall be selected such that for the relevant polarization (TE and/or TM) the etched input and output regions $z < 0$, $z > L$ of the device constitute single mode waveguides, while the strip region in between supports two guided modes.

Then a rough simulation of the light propagation in terms of a 2–D overlap model requires only a few ingredients. ψ denotes the guided mode profile of the input and output segments. ϕ_0, ϕ_1 and β_0, β_1 are the fundamental and first order mode of the thick coupling section and the corresponding propagation constants. The modes are meant to be normalized with respect to a proper scalar product $(\ .\ ,\ .\ )$; see Ref. 1 for a specification of the abstract notation. Assuming that a normalized input field passes a thick segment of length L, by equating transverse components at the two waveguide junctions, projecting on the involved fields, and using the orthogonality properties for guided modes, one arrives at the following expression for the relative power transmission:

$$\mathcal{P}(L) = w_0^2 + w_1^2 + 2w_0 w_1 \cos(\beta_0 - \beta_1)L\,. \tag{1}$$

The squared mode overlaps $w_j = (\psi, \phi_j)^2$ are real for suitably chosen basic mode profiles.

The transmitted power varies strictly harmonically with respect to the length L of the strip segment, with a half beat length or coupling length $L_\mathrm{c} = \pi/(\beta_0 - \beta_1)$. Obviously the maximum respectively minimum throughput is given by the sum $(w_0 + w_1)^2$ or the difference $(w_0 - w_1)^2$ of the overlaps. Hence one can expect interferometric behaviour of the device — i.e. alternatively almost complete or no power transmission — if the geometric parameters can be adjusted such that the overlaps are equal, while at the same time their sum is as large as possible. For the applications discussed in Section 4 and Section 5, the condition $w_0 = w_1$, implying the complete suppression of the power transmission, is essential. Figure 2 shows examples for the involved mode profiles and their superpositions, for a configuration where this condition is met.

For a properly adjusted geometry a symmetric superposition of ϕ_0 and ϕ_1 can be reasonably close to the input and output mode ψ. Therefore little power is lost, if this field excites the strip region at $z = 0$, or if the symmetric superposition arrives at the output junction in $z = L$. At the same time, the antisymmetric superposition of ϕ_0 and ϕ_1, with absolute values of the amplitudes as before, but with an additional phase difference of π, is orthogonal to ψ. Hence the output mode does not receive any power, if this superposition excites the lower region at $z = L$.

To check these statements, we employed a more rigorous mode expansion technique[3,4] as formulated in Ref. 1. The calculations take the reflected and radiated parts of the electromagnetic fields explicitely into account. Figure 3 shows the results. The input mode ψ transits smoothly into the strip segment, with hardly any radiation visible (a). Likewise one observes a smooth transition from the thick to the thin segment, if the proper superposition of ϕ_0 and ϕ_1 hits the output junction (b). On the contrary, the antisymmetric superposition of ϕ_0 and ϕ_1 is not able to excite the output mode ψ at all (c). In that case the power is partly reflected, but mostly radiated away, a smaller part into the cover, a larger fraction into the higher index substrate.

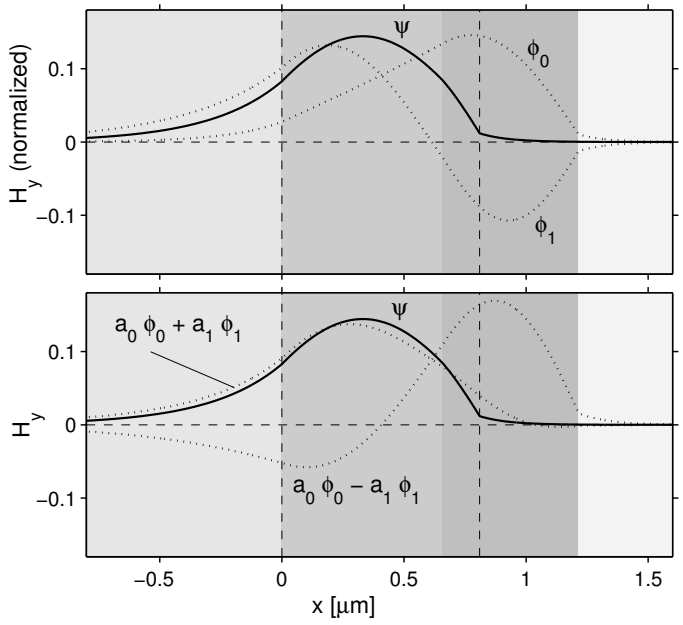

Figure 2. Basic magnetic field component H_y of the TM modes for the structure of Figure 1, with parameters $t = 1.215\,\mu$m, $b = 0.656\,\mu$m, $h = 0.405\,\mu$m, $n_{\rm c} = 1.0$, $n_{\rm t} = 2.275$, $n_{\rm b} = 2.157$, $n_{\rm s} = 1.95$, and $\lambda = 1.3\,\mu$m. Top: The mode ψ of the lower core, and the profiles ϕ_0, ϕ_1 of the strip region. Bottom: With suitable amplitudes $a_j = \sqrt{w_j} = 0.703$, the modes of the thicker waveguide form a field that matches the output mode well (+), or that is orthogonal to the output profile (−). The dashed vertical lines mark the boundaries of the input/output core, while the shading indicates the permittivity of the thick strip segment.

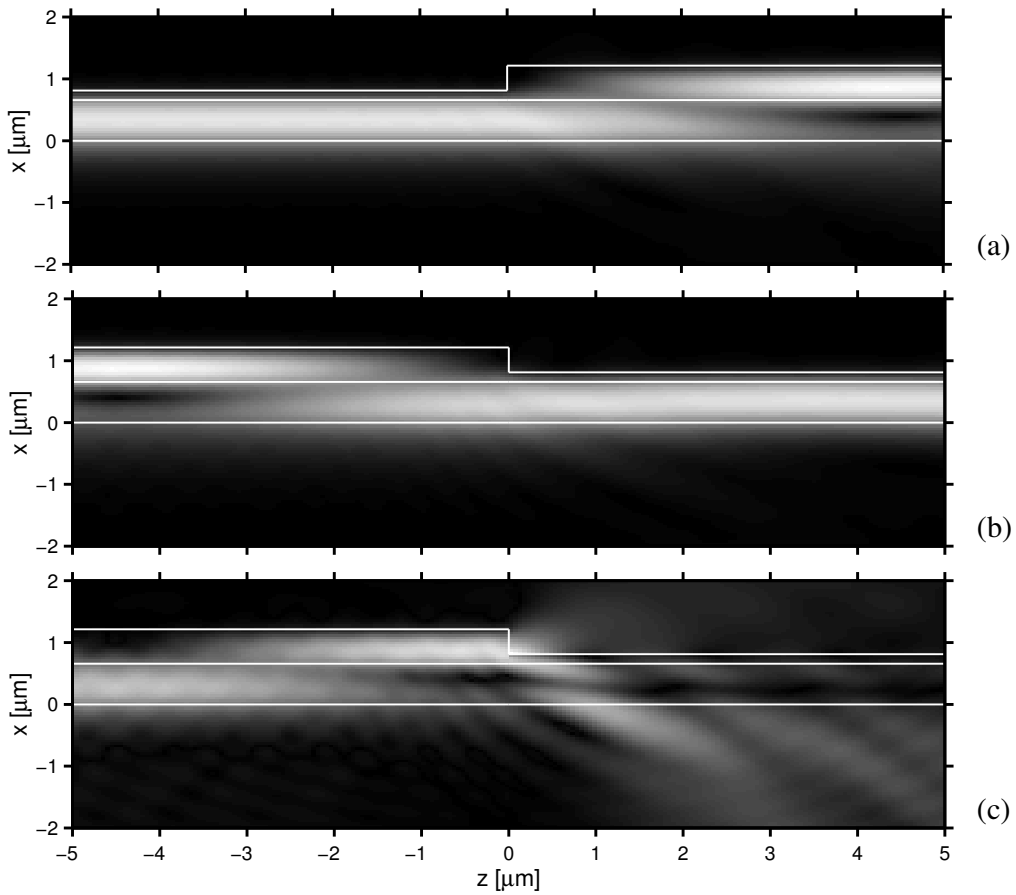

Figure 3. Simulations of the light propagation through the isolated junctions, for parameters as given in the caption of Figure 2. The gray scale levels correspond to the squareroot of the z-component of the local Poynting vector. (a) Transition from the thin to the thick segment; Input: the single mode of the thin segment. (b)/(c) Transition from the thick to the thin segment; Input: the superposition of the two guided modes of the thick segment with the positive/negative sign (see Figure 2(b)). Here 'input' means that the two modes are launched to arrive at the junction with equal amplitudes and proper phases. The z-coordinates displayed in (b) and (c) indicate the distance from the junction at $z = L$.

The difference between (b) and (c) can be explained only partly by the shift of the location of the impinging field from the lower (b) to the upper waveguide region (c). For the situation (c) of the destructive interference, Figure 2(b) shows a considerable amount of the incoming field $a_0\phi_0 - a_1\phi_1$ in the region $x < t - h$ of the outgoing waveguide. Reasoning in terms of orthogonality of the involved fields is inevitable in this case.

(a) Input: ψ

	$\psi, \rightarrow$	$\psi, \leftarrow$	$\phi_0, \rightarrow$	$\phi_0, \leftarrow$	$\phi_1, \rightarrow$	$\phi_1, \leftarrow$
ME	1	$1.1 \cdot 10^{-6}$	0.49	0	0.50	0
FDTD	1	$3.0 \cdot 10^{-5}$	0.48	0	0.51	0

(b) Input: $(\phi_0 + \phi_1)/\sqrt{2}$

	$\phi_0, \rightarrow$	$\phi_0, \leftarrow$	$\phi_1, \rightarrow$	$\phi_1, \leftarrow$	$\psi, \rightarrow$	$\psi, \leftarrow$
ME	1/2	$2.1 \cdot 10^{-4}$	1/2	$1.1 \cdot 10^{-4}$	0.99	0
FDTD	1/2	$5.0 \cdot 10^{-4}$	1/2	$3.0 \cdot 10^{-4}$	0.99	0

(c) Input: $(\phi_0 - \phi_1)/\sqrt{2}$

	$\phi_0, \rightarrow$	$\phi_0, \leftarrow$	$\phi_1, \rightarrow$	$\phi_1, \leftarrow$	$\psi, \rightarrow$	$\psi, \leftarrow$
ME	1/2	$2.0 \cdot 10^{-2}$	1/2	$1.3 \cdot 10^{-2}$	$6.5 \cdot 10^{-5}$	0
FDTD	1/2	$3.6 \cdot 10^{-2}$	1/2	$2.8 \cdot 10^{-2}$	$9.0 \cdot 10^{-4}$	0

Table 1. Relative guided mode powers for the simulation of isolated waveguide junctions corresponding to the plots of Figure 3. Rows ME list the values computed with a rigorous mode expansion technique[1], the rows FDTD contain the results of finite difference time-domain beam propagation simulations[5]. Arrows $\rightarrow$ mark incident resp. transmitted fields, propagating in the positive z-direction. Reflected fields are indicated by the symbol $\leftarrow$.

For a more quantitative assessment, Table 1 lists the squared relative amplitudes of the guided modes that are relevant in the three configurations of Figure 3. The table compares results of two completely independent rigorous techniques[1,5]. Agreeing reasonably, the values confirm the estimations of the simple overlap technique, that is sketched at the beginning of this section, surprisingly well. The overlap calculations, which actually led to the parameters of Figures 2, 3 and Table 1, predict equal ongoing mode powers $\phi_j, \rightarrow$ of 0.49 for (a), a unit transmission $\psi, \rightarrow$ for (b), and a vanishing transmission $\psi, \rightarrow$ in case (c). Despite the abrupt strip edges, Table 1 justifies also the approximation of neglecting reflections entirely. As exemplified in the following sections, one can expect Eq. (1) to yield useful guidelines for the design of devices based on the cross strip geometry.

3. OPTIMIZED INTERFEROMETER GEOMETRIES

While the calculations of the preceding section refer to the double layer configuration of Figure 1, the arguments hold for simpler single layer structures ($b = 0$) as well[1]. In general, when designing an interferometer device on the basis of the present concept, there is some freedom in the choice of the dielectric layering. According to the overlap model, some conditions have to be observed, including the requirement of single mode port segments, of a bimodal strip segment, and in particular the vanishing overlap difference. Once the operation wavelength and the available materials are fixed, the task is to find suitable thicknesses t, b, and a suitable etching depth h. We have observed that the conditions mentioned above do not uniquely specify these parameters; hence the remaining freedom can be used to optimize the maximum throughput power, i.e. the dynamic range of the device.

Figures 4 to 7 compare the achievable interferometer performance, measured in terms of this maximum power transmission, for some characteristic single layer (Figure 4) and double layer systems. The fixed parameters resemble typical values for Silicon-Nitride / Silicon-Oxide materials[6].

According to Figure 4, interferometer operation is possible for a simple single layer strip. For low loss performance, the structure has to be strongly asymmetric; at least for the present material system even the smallest cover refractive index of 1.0 leads to moderate maximum power transmission of about 90 % only. The shape of the curve suggests that a structure with higher substrate and film refractive index would be advantageous. A proper interferometer can not be constructed on the basis of a symmetric single layer waveguide with equal substrate and cover refractive index.

The optimum structure of Figure 4, the air covered waveguide, can be significantly improved, if one uses an additional upper guiding layer with increased refractive index. This is shown in Figure 5. For $n_\mathrm{t} > 2.31$, the maximum transmission is larger than 99 % for both TE and TM polarization. Note that Figure 5 starts at $n_\mathrm{t} = 2.05$, hence the left borders of Figure 4 and Figure 5 can not be compared directly (When Figure 5 is extended towards $n_\mathrm{t} = 2.01$, the parameter b loses its meaning and another optimum appears in $\mathcal{P}_{\max}(t, h)$, which corresponds to the point $n_\mathrm{c} = 1$ in Figure 4.).

Although Figures 4 and 5 give evidence that a low cover refrative index is desirable, e.g. for reasons of protecting an integrated optical circuit a cladding may be required, which usually has a higher refractive index than air. Corresponding configurations are considered in Figures 6 and Figure 7. As before, a certain asymmetry in the layering is necessary to enable interferometer performance, which is easier to achieve (in terms of refractive index contrast) for a bottom film layer

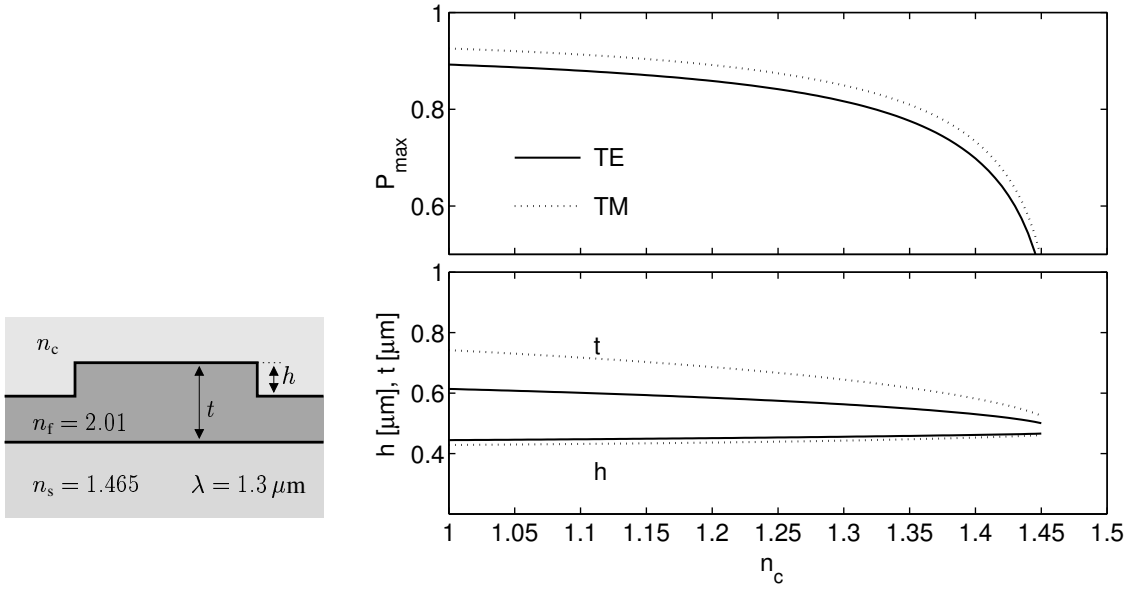

Figure 4. Optimized geometries for interferometers based on a single guiding layer with upper cladding, versus the refractive index of the cladding layer. For the parameters stated in the left inset, the thicknesses t and etching depths h, that are plotted in the lower part, yield vanishing minimum transmission $(w_0 - w_1)^2 = 0$ and optimal maximum power throughput $\mathcal{P}_{\text{max}} = (w_0 + w_1)^2$, which is shown in the upper plot. The continuous curves correspond to TE polarization, the dotted lines apply to TM polarized fields.

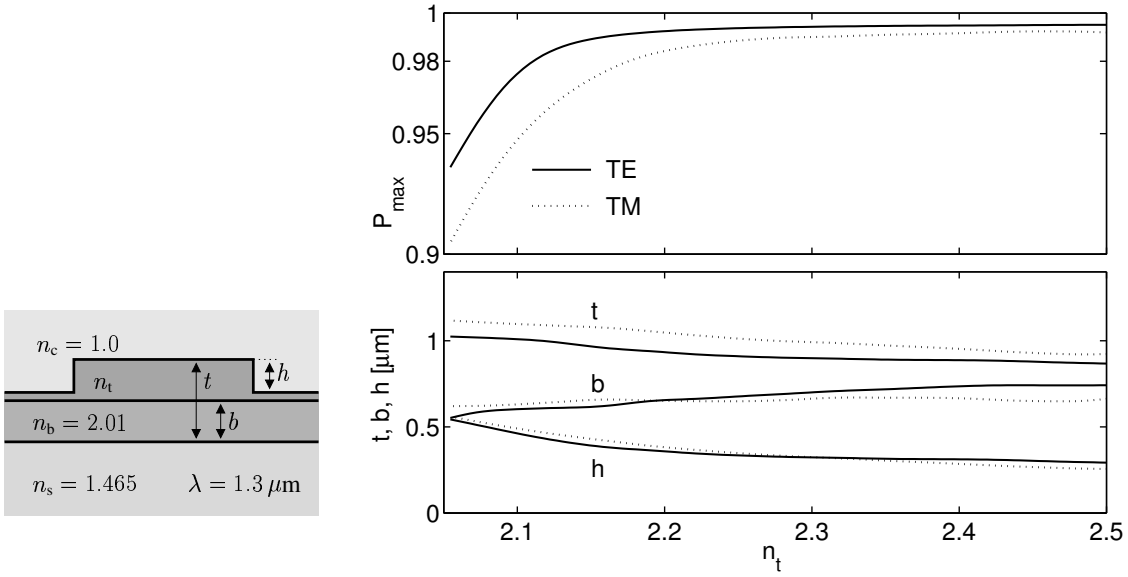

Figure 5. Analogon to Figure 4, for double layer waveguides with variable refractive index of the top film layer. The structure is covered by air.

with lower refractive index, as in Figure 7. Compared to Figure 6 with only moderate performance for TM polarized fields, the optimized quantities for the less strongly guiding structures of Figure 7 show a less pronounced polarization dependence, and upper throughput levels of about $98\,\%$ for both TE and TM polarization.

The plots of this section were intended to establish some general notion about the achievable interferometer performance and some design aspects. Concrete applications will usually introduce other constraints, such that the resulting devices do not correspond directly to one of the optimized structures in Figures 4 to Figure 7. But usually the specific application leaves also some design freedom, which can be exploited to optimize the interferometer aspects of the device. This is the case for the examples shown in the next section.

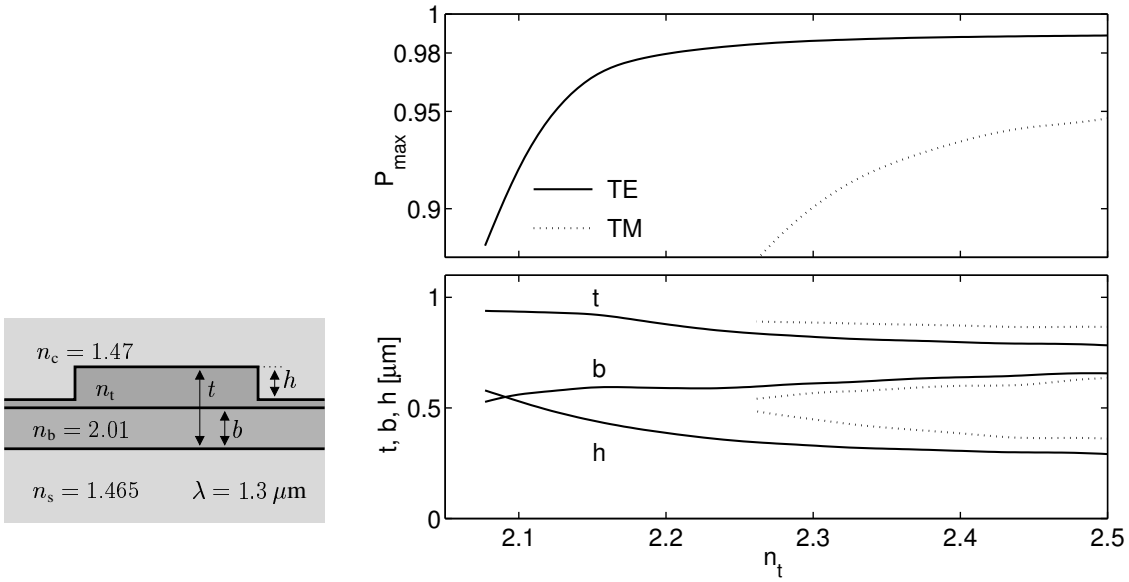

Figure 6. Analogon to Figure 5, for an upper cladding with a refractive index that is similar to the substrate value.

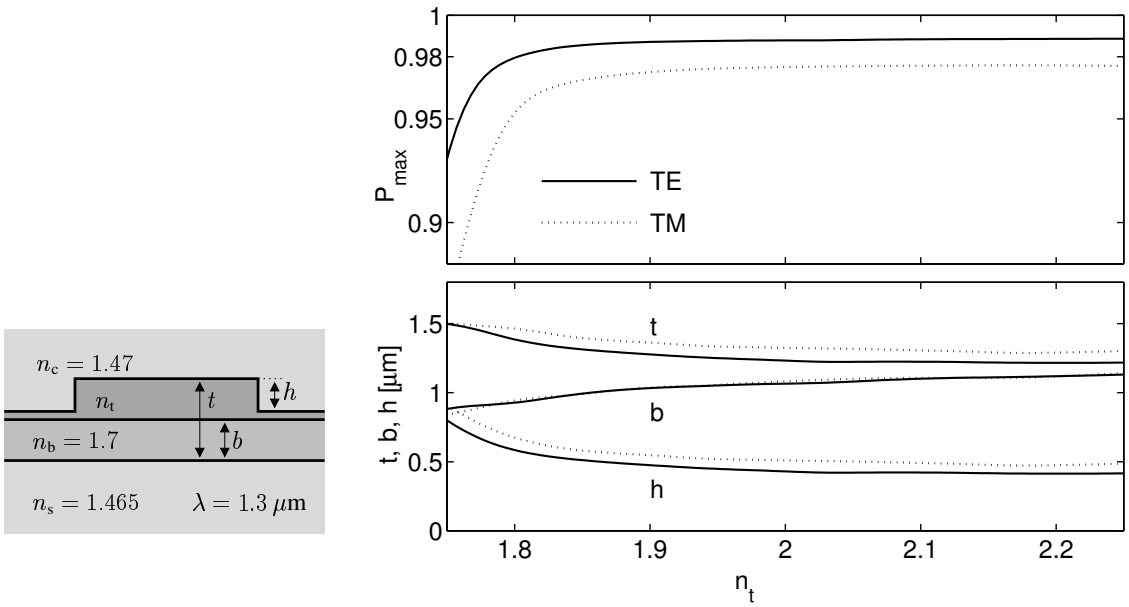

Figure 7. Analogon to Figure 6, now for a lower refractive index of the bottom film layer. Note the different relevant intervals of n_t in Figures 6 and 7.

4. POLARIZER DEVICE

Owing to the birefringent properties of almost all dielectric guiding structures, a large variety of concepts has been developed for polarization discrimination in integrated optics. Most proposals for guided wave polarizers rely on trying to exclusively attenuate one of the basic TE or TM fields, where the damping mechanisms are manifold, including isotropic absorption[7], dichroism[8], or strong birefringence[9]. In turn, polarization splitters are usually interferometric devices. Several different types have been investigated, e.g. Mach-Zehnder structures[10] or directional couplers[11]. As an alternative, we propose to use the geometry of Figure 1 to construct a simple interferometric polarizer.

A TE-pass-polarizer, i.e. a device that transmits as much as possible of the TE input power while it blocks the TM throughput, has to be assessed in terms of the polarization discrimination or extinction ratio $\mathrm{ER} = 10\log_{10}\mathcal{P}^{\mathrm{TE}}/\mathcal{P}^{\mathrm{TM}}$ and the insertion loss $\mathrm{LO} = -10\log_{10}\mathcal{P}^{\mathrm{TE}}$, where $\mathcal{P}^{\mathrm{TE}}$ and $\mathcal{P}^{\mathrm{TM}}$ are the relative TE and TM power transmissions (1).

Given the material parameters and the wavelength, a proper total thickness t, bottom layer thickness b, and strip width L are to be identified. Eq. (1) predicts periodic variations of $\mathcal{P}^{\mathrm{TE}}$ and $\mathcal{P}^{\mathrm{TM}}$ with different beat lengths L_c^{TE} and L_c^{TM}. Polarizer

performance requires a (short) configuration, where L is an even multiple of L_c^TE and simultaneously an odd multiple of L_c^TM. For a difference of one in the multiplicities, these conditions fix the optimum polarizer length as

$$L_\mathrm{p} = \frac{L_\mathrm{c}^\mathrm{TE} L_\mathrm{c}^\mathrm{TM}}{L_\mathrm{c}^\mathrm{TE} - L_\mathrm{c}^\mathrm{TM}} \,. \tag{2}$$

By varying t and b over the range where the strip segment supports two guided modes for both polarizations, evaluating L_p and checking for an even integer $L_\mathrm{p}/L_\mathrm{c}^\mathrm{TE}$, one can indeed find a set of suitable geometries, specified by pairs of values t, b. The parameters of Table 2 lead to $L = L_\mathrm{p} = 6L_\mathrm{c}^\mathrm{TE} = 7L_\mathrm{c}^\mathrm{TM}$. For each pair t, b, a suitable etching depth h can be identified, where the condition of $w_0^\mathrm{TM} = w_1^\mathrm{TM}$ for destructive interference is met for TM waves. The design is completed by selecting the geometry that yields the maximum TE power transmission $(w_0^\mathrm{TE} + w_1^\mathrm{TE})^2$.

	t	b	h	L	λ	n_s	n_b	n_t	n_c
q	$0.673\,\mu$m	$0.444\,\mu$m	$0.339\,\mu$m	$10.882\,\mu$m	$1.3\,\mu$m	1.465	2.01	2.3	1.0
Δq	26 nm	9 nm	18 nm	100 nm	20 nm	0.007	0.009	0.024	0.08

Table 2. Structural parameters for a planar polarizer as sketched in Figure 1. The tolerances Δq indicate that the polarizer should still achieve an extinction ratio higher than 20 dB and introduce losses below 1 dB, if a single parameter deviates from the optimum value q by no more than $\pm\Delta q$.

Table 2 summarizes the parameters of the resulting polarizer proposal. For the tuned device, a rigorous mode expansion simulation predicts relative power throughputs of $\mathcal{P}^\mathrm{TE} = 97\,\%$ and $\mathcal{P}^\mathrm{TM} = 0.09\,\%$. This amounts to a polarization discrimination of about ER $= 30$ dB and an insertion loss LO $= 0.1$ dB*. Relative guided powers of $0.1\,\%$ (TE) and $3.3\,\%$ (TM) are reflected. Plots of the corresponding fields in Figure 8 illustrate the behaviour of the interferometer.

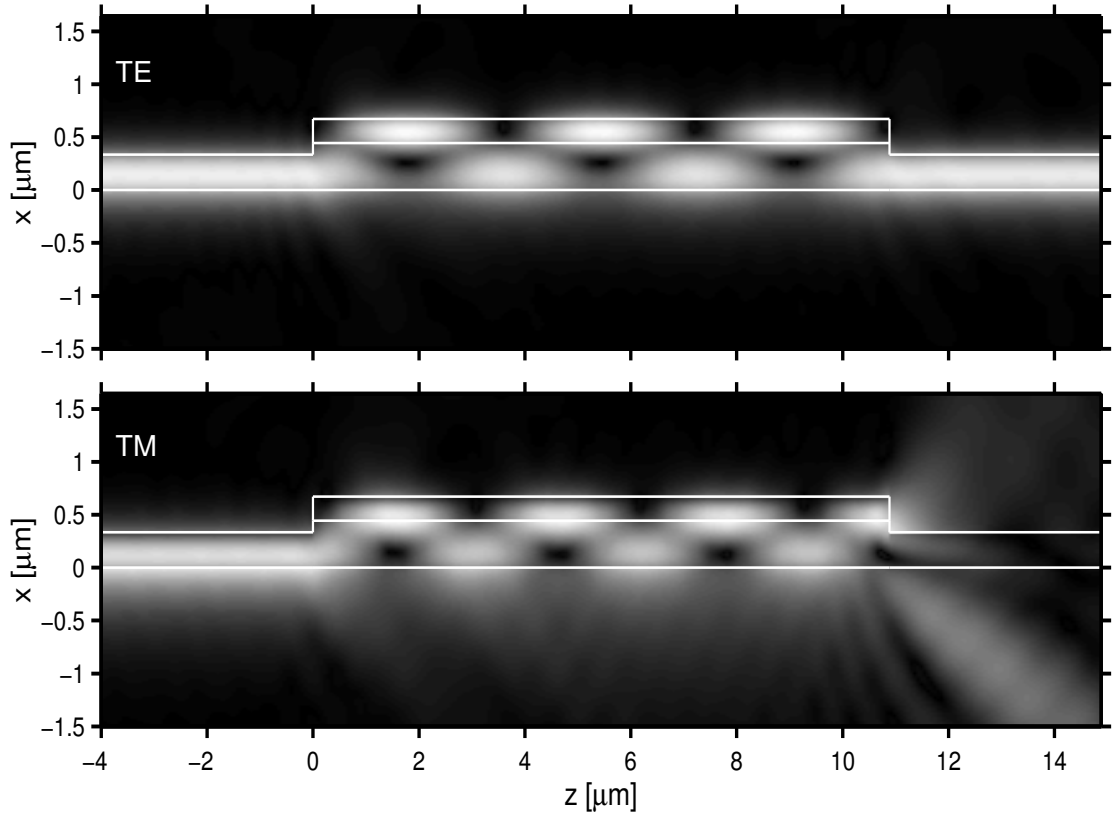

Figure 8. Simulation of the light propagation through the cross strip defined by Table 2, for TE (top) and TM polarized input (bottom). For TM polarization, the output junction scatters almost the entire power into the surrounding, while TE polarized waves pass the device smoothly.

*For comparable material parameters, the single layer design proposed in Ref. 1 achieves a maximum TE transmission of $93\,\%$ or minimum loss of 0.3 dB.

The simple polarizing strip may help to overcome some of the drawbacks of the polarizer concepts mentioned before: It requires neither exotic materials nor complicated processing steps. The design is adaptable to a certain range of material and wavelength parameters. Together with reasonable levels of polarization discrimination and insertion loss and an extremely short length, the cross strip geometry should be a promising candidate for including polarizer functionality into a larger integrated optical circuit.

5. CONCEPT FOR AN ISOLATOR EXPERIMENT

Optical isolators are intended to pass the optical power in one direction of light propagation while blocking the power transmission for the opposite direction. At present, experimental realizations in an integrated optical setting are still rare. Analogously to their micro- or bulk-optic counterparts, many concepts for integrated devices rely on the Faraday-effect, the nonreciprocal polarization conversion caused by a magnetooptic material with the magnetization oriented parallel to the direction of light propagation[12]. If the magnetization is adjusted perpendicularly to that direction, the magnetooptic anisotropy shows up in different phase velocities of counterpropagating waves, the nonreciprocal phase shift. A number of isolator concepts based on nonreciprocal interferometry rely on these phase shifts; see e.g. Refs. 13–15 for recent proposals.

In this section we address the task by means of the cross strip geometry, with the guiding layers made of magnetooptical materials. Figure 9 shows the relevant structure; a more elaborate assessment of the present proposal is given in Ref. 2. Avoiding the necessity to include polarizers, power splitters, or laterally precisely dimensioned (bend) waveguides, the nonreciprocal cross strip should be superiour to many of the previous concepts with respect to manufacturing effort.

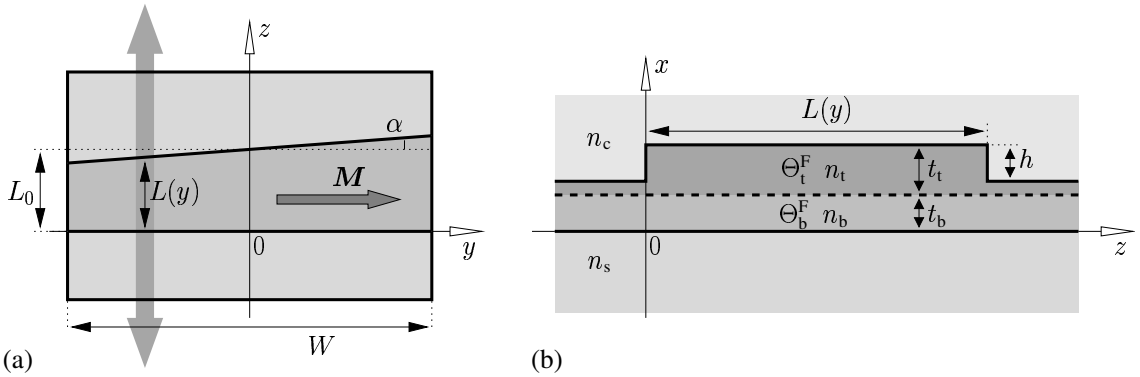

Figure 9. Top view (a) and x-z-cut (b) of the magnetooptic cross strip interferometer. The double layer waveguide with film thicknesses t_b and t_t consists of two magnetooptic layers with opposite Faraday rotations $\Theta_\mathrm{b}^\mathrm{F}$ and $\Theta_\mathrm{t}^\mathrm{F}$, with the magnetization $\boldsymbol{M}$ oriented along the y-axis. The front and back edges of the strip of width W are adjusted at a small angle α. A beam injected at position y passes through a strip segement of length $L(y)$.

Besides the guiding refractive index, there is a second contribution to the permittivity, which accounts for the magnetooptic properties of the film material. With the static magnetization oriented in the film plane perpendicular to the direction of light propagation, the primary effects of this magnetooptic anisotropy are nonreciprocal phase shifts for TM polarized fields†, i.e. the propagation constants for modes propagating in positive and negative z-direction differ[16]. If relevant, superscripts $d = \mathrm{f}, \mathrm{b}$ for forward and backward propagation specify the direction. While in principle this applies to propagation constants as well as to mode profiles, by computing the exact analytical mode solutions for the magnetooptic waveguide[17] one observes that the small change of the mode profiles with the direction of propagation is clearly negligible. Thus the magnetooptic effect can be modeled adequately in the framework of perturbation theory[18], using the mode profiles of the basic isotropic structure. We show below that the angled strip geometry, together with limited beam width, allows to meet the critical condition for isolator performance, which will be established in the next paragraph.

Along with the propagation constants β_0^d, β_1^d, the coupling lengths L_c^d differ for forward and backward transmission, and one can expect a nonreciprocal behaviour of the power throughput as well: $\mathcal{P}^\mathrm{f} \neq \mathcal{P}^\mathrm{b}$. The isolator device has to be assessed in terms of the isolation ratio $\mathrm{IS} = 10\log_{10}\mathcal{P}^\mathrm{f}/\mathcal{P}^\mathrm{b}$ and loss $\mathrm{LO} = -10\log_{10}\mathcal{P}^\mathrm{f}$. Hence for optimal performance, the length L of the strip segment should match at the same time an even multiple of the forward coupling length and an odd multiple of the backward coupling length: $L = 2mL_\mathrm{c}^\mathrm{f} = (2m \pm 1)L_\mathrm{c}^\mathrm{b}$. This allows to compute a characteristic length

$$L_\mathrm{is} = \frac{L_\mathrm{c}^\mathrm{f} L_\mathrm{c}^\mathrm{b}}{|L_\mathrm{c}^\mathrm{f} - L_\mathrm{c}^\mathrm{b}|} = \frac{\pi}{|(\beta_0^\mathrm{f} - \beta_0^\mathrm{b}) - (\beta_1^\mathrm{f} - \beta_1^\mathrm{b})|} \tag{3}$$

†TE waves are not affected in this configuration, therefore all following considerations apply only to TM polarized fields.

for the isolating interferometer. A short device needs the difference between the forward and backward coupling lengths to be large. According to the second equality, this requires a pronounced difference in the nonreciprocal phase shifts $\beta_j^{\mathrm{f}} - \beta_j^{\mathrm{b}}$ of the two modes. Therefore, our design rests on a double layer structure with opposite signs of the Faraday rotation in the two magnetooptic films. If t_{b} and t_{t} are selected such that the central boundary at $x = t_{\mathrm{b}}$ is placed close to the field maximum of ϕ_0, or close to the zero of ϕ_1, respectively, the fundamental mode is subject to a large nonreciprocal phase shift, while the first order mode remains almost unaffected by the magnetooptic perturbation. See e.g. Ref. 16 for details on the optimization of the effect.

Analogously to the polarizer design, this is one of the constraints mentioned at the end of Section 3 that fixes already some of the geometric parameters of the cross strip device, in this case the layer thicknesses t_{b}, t_{t}, and, via Eq. (3), the basic strip width $L_0 = L_{\mathrm{is}}$. Only h remains to be selected such that the condition $w_0 = w_1$ for complete destructive interference is met. Fortunately the properties of the garnet materials are such that a suitable etching depth exists. With the slightly higher refractive index of the upper film, the layering, determined by the objective of a short device, yields in fact an interferometer with excellent performance.

Although optimized for minimum size, for the currently available magnetooptic materials with small specific Faraday-rotation the strip has to be several millimeters long. The isolating interferometer of Table 3 will have to distinguish between 1258 forward half-beats and 1259 coupling lengths in the backward direction. This necessarily requires a postfabrication tuning possibility, which for the present proposal can be found in the lateral beam incoupling position y. We refer now to Figure 9(a). Assume that the lateral extension of the device W, the basic strip width L_0, and the strip angle α are selected such that the interval $[L_0 - (W/2)\tan\alpha, L_0 + (W/2)\tan\alpha]$ includes a few coupling lengths around $L_0 = L_{\mathrm{is}}$. For the present parameters, angles α between $0.01°$ and $0.1°$ are suitable. Then the light that is coupled in at position y passes a cross strip interferometer of length $L(y) = L_0 + y\,\tan\alpha$. By shifting the incoupling position on a millimeter scale, one can always prepare a configuration where the isolator performance is in a local maximum[2].

By 'tolerances' we denote deviations of single parameters, which are allowed such that the experiment can be carried out successfully, i.e. where one can exceed certain limits for isolation and loss by shifting the input focus. The values Δq are estimated such that a performance with IS $\geq$ 20 dB and LO $\leq$ 1 dB can be reached after tuning the device, provided that a parameter q deviates by no more that $\pm\Delta q$ from its optimum value.

Table 3 summarizes a set of reasonable isolator parameters and the corresponding tolerances. Note that 'loss' refers to the field mismatch at the waveguide junctions only. For a real device, material absorption, incoupling losses, etc. would have to be added. In the framework of the present overlap model, for tuned parameters the experiment should achieve an ideal isolation and an insertion loss of only $\mathrm{LO}_{\mathrm{min}} = 0.09$ dB. The nonreciprocal effect results in slightly different coupling lengths of $L_{\mathrm{c}}^{\mathrm{f}} = 4.5008\,\mu$m and $L_{\mathrm{c}}^{\mathrm{b}} = 4.4973\,\mu$m for opposite directions of propagation.

	t_{b}	t_{t}	h	L_0	λ	n_{s}	n_{b}	n_{t}	n_{c}	$\Theta_{\mathrm{b}}^{\mathrm{F}}$	$\Theta_{\mathrm{t}}^{\mathrm{F}}$
q	$0.656\,\mu$m	$0.559\,\mu$m	$0.405\,\mu$m	5.663 mm	$1.3\,\mu$m	1.950	2.157	2.275	1.0	$150°/\,$cm	$-1000°/\,$cm
Δq	$\geq 0.2\,\mu$m	$0.16\,\mu$m	30 nm	1.6 mm	≥ 90 nm	0.1	0.02	0.02	≥ 0.4	$202°/\,$cm	$360°/\,$cm

Table 3. Structural parameters q and fabrication tolerances Δq for a cross strip isolator experiment as sketched in Figure 9. Δq corresponds to limits for isolation and loss of 20 dB and 1 dB. See the text for a concise interpretation of the limits for the parameter deviations.

The proposed tuning mechanism allows to compensate deviations in the film thicknesses, etching depth, the strip width, and in the material parameters that occur during the fabrication process. In principle it allows also to correct a drift of the (constant) wavelength that is applied in the experiment; the tolerance value $\Delta\lambda$ in Table 3 refers to that setting. However, for an application in a telecommunication setup, the *fixed* device has to work for a certain frequency range; any tuning technique can adjust optimum performance for a specific central wavelength only. For a tuned device according to Table 3, a plot of the isolation and loss versus the wavelength[2] shows that proper operation can be expected in an interval of about 8 nm width around the design wavelength of $1.3\,\mu$m, if one demands an isolation level above 20 dB. This wavelength range will be relevant for the final application.

We have checked the former considerations by rigorous mode expansion modeling[1,2]. Figure 10 illustrates the intensity distributions around the waveguide discontinuities for the two directions of light propagation. For the tuned setup with parameters as given in Table 3, the simulations predict a relative forward power transmission of 98 % and a relative reflected power of 0.03 %. In the blocking direction, a relative power of 0.27 % passes the device and a power fraction of 0.03 % is reflected. This amounts to an isolation ratio of 26 dB; the device suffers from forward losses of 0.1 dB.

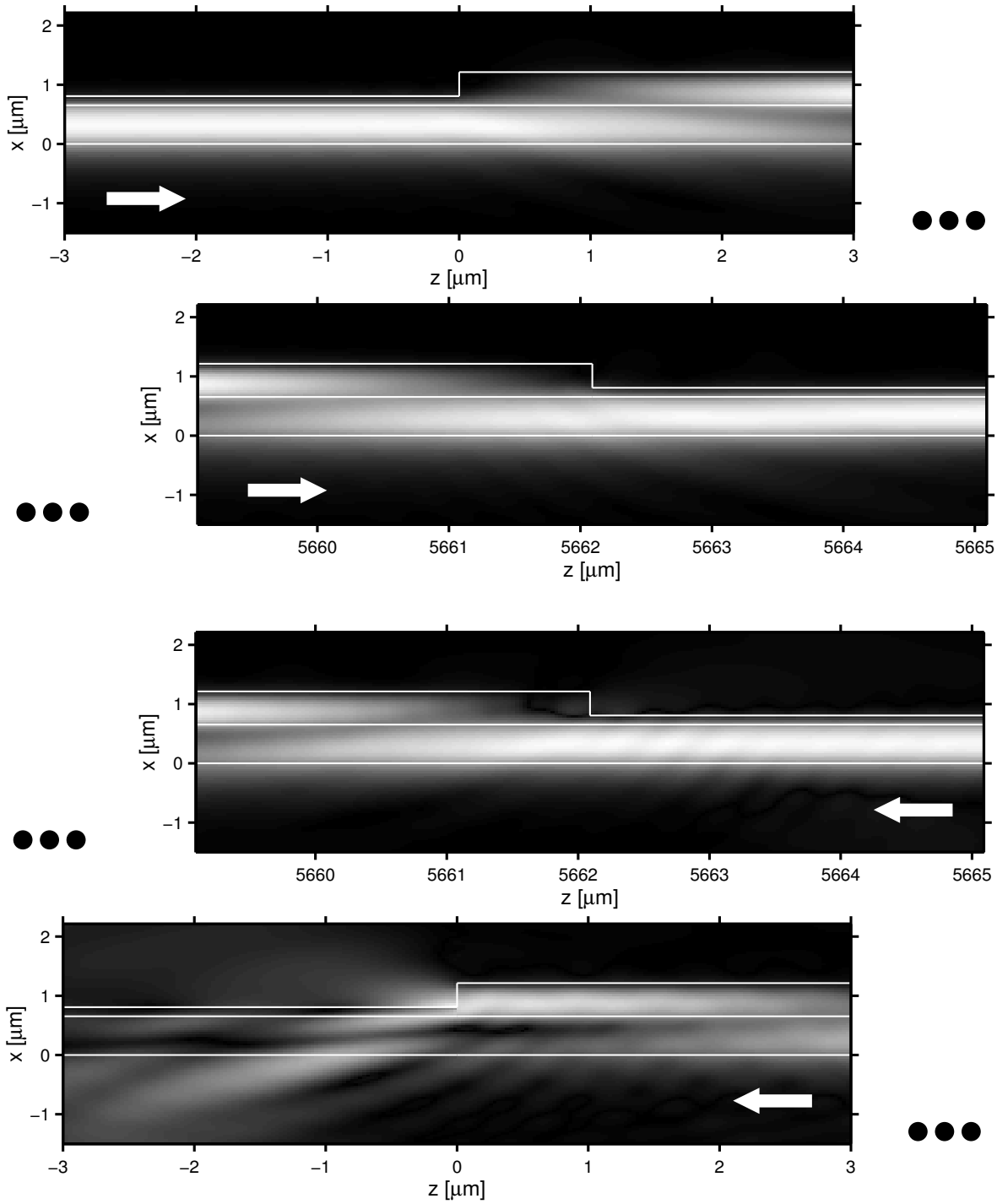

Figure 10. Simulation of the forward (top) and backward (bottom) light propagation through an isolating cross strip as prescribed by Table 3, with a length of $L = 5.662\,\mathrm{mm}$. In forward direction, almost the entire power passes the device, while the junction at $z = 0$ scatters backward propagating waves into the surrounding.

6. CONCLUSIONS

A specific class of waveguide interferometers, where a beam of light traverses a deeply etched rib perpendicularly, turns out to be very promising for the realization of explicitely simple integrated optical devices. The theoretical modeling is possible in a quasianalytical framework of eigenfunction expansions, verified by rigorous FDTD calculations. While basic interferometer functionality can be obtained with single layer dielectric films, asymmetric double layer configurations show advantages with respect to optical losses. Until now, we have proposed and simulated concrete concepts for polarizer devices and a magnetooptic isolator setup; experimental realizations are under way for both concepts. An extension of the present planar model to more realistic channel waveguides is desired, as well as an elaboration of the concept towards other functionalities.

REFERENCES

1. M. Lohmeyer and R. Stoffer, "Integrated optical cross strip polarizer concept," *Optical and Quantum Electronics* , 2000. Accepted for publication.
2. M. Lohmeyer, L. Wilkens, O. Zhuromskyy, H. Dötsch, and P. Hertel, "Integrated magnetooptic cross strip isolator," *Optics Communications* , 2000. Submitted.
3. G. Sztefka and H. P. Nolting, "Bidirectional eigenmode propagation for large refractive index steps," *IEEE Photonics Technology Letters* **5**(5), pp. 554–557, 1993.
4. J. Willems, J. Haes, and R. Baets, "The bidirectional mode expansion method for two-dimensional waveguides: the TM case," *Optical and Quantum Electronics* **27**, pp. 995–1007, 1995.
5. R. Stoffer, H. J. W. M. Hoekstra, R. M. de Ridder, E. van Groesen, and F. P. H. van Beckum, "Numerical studies of 2D photonic crystals: Waveguides, coupling between waveguides and filters," *Optical and Quantum Electronics* **32**, pp. 947–961, 2000.
6. K. Wörhoff, P. V. Lambeck, H. Albers, O. F. J. Noordman, N. F. van Hulst, and T. J. A. Popma, "Optimization of LPCVD Silicon Oxynitride growth to large refractive index homogeneity and layer thickness uniformity," in *Micro-optical Technologies for Measurement, Sensors, and Microsystems II*, O. M. Parriaux, E. B. Kley, B. Culshaw, and M. Breidne, eds., vol. 3099 of SPIE Proceedings, pp. 257–268, 1997.
7. M. Saini, E. K. Sharma, and M. Singh, "Strong effect of output coupling on the performance of metal-clad waveguide polarizers," *Optics Letters* **20**(4), pp. 365–367, 1995.
8. M. J. Bloemer and J. W. Haus, "Broadband waveguide polarizers based on the anisotropic optical constants of nanocomposite films," *Journal of Lightwave Technology* **14**(6), pp. 1534–1540, 1996.
9. C. S. Pérez, A. Morand, P. Benech, S. Tedjini, D. Bosc, and A. Rousseau, "Low cost integrated optical polarizer with an hybrid structure of birefringent polymer and ion-exchanged glass waveguide," in *Integrated Optics Devices III*, G. C. Righini and S. I. Najafi, eds., vol. 3620 of SPIE Proceedings, pp. 118–125, 1999.
10. Y. Shani, C. H. Henry, R. C. Kistler, and K. J. Orlowsky, "Four-port integrated optic polarization splitter," *Applied Optics* **29**(3), pp. 337–339, 1990.
11. M. Lohmeyer, N. Bahlmann, O. Zhuromskyy, and P. Hertel, "Radiatively coupled waveguide polarization splitter simulated by wave-matching based coupled mode theory," *Optical and Quantum Electronics* **31**, pp. 877–891, 1999.
12. M. Lohmeyer, N. Bahlmann, O. Zhuromskyy, H. Dötsch, and P. Hertel, "Phase-matched rectangular magnetooptic waveguides for applications in integrated optics isolators: numerical assessment," *Optics Communications* **158**, pp. 189–200, 1998.
13. J. Fujita, M. Levy, R. M. Osgood, L. Wilkens, and H. Dötsch, "Waveguide optical isolator based on Mach-Zehnder interferometer," *Applied Physics Letters* **76**(16), pp. 2158–2160, 2000.
14. M. Fehndrich, A. Josef, L. Wilkens, J. Kleine-Börger, N. Bahlmann, M. Lohmeyer, P. Hertel, and H. Dötsch, "Experimental investigation of the nonreciprocal phase shift of a TE-mode in a magneto-optic rib waveguide," *Applied Physics Letters* **74**(20), pp. 2918–2920, 1999.
15. O. Zhuromskyy, H. Dötsch, M. Lohmeyer, L. Wilkens, and P. Hertel, "Magneto-optical waveguides with polarization independent nonreciprocal phase shift," *Journal of Lightwave Technology* , 2000. Submitted.
16. M. Wallenhorst, M. Niemöller, H. Dötsch, P. Hertel, R. Gerhardt, and B. Gather, "Enhancement of the nonreciprocal magneto-optic effect of TM modes using iron garnet double layers with opposite Faraday rotation," *Journal of Applied Physics* **77**(7), pp. 2902–2905, 1995.
17. H. Dötsch, P. Hertel, B. Lührmann, S. Sure, H. P. Winkler, and M. Ye, "Applications of magnetic garnet films in integrated optics," *IEEE Transactions on Magnetics* **28**(5), pp. 2979–2984, 1992.
18. M. Shamonin and P. Hertel, "Analysis of non-reciprocal mode propagation in magneto-optic rib-waveguide structures with the spectral-index method," *Applied Optics* **33**(27), pp. 6415–6421, 1994.